# Two-photon retinal theranostics by adaptive compact laser source

Podlipec, R.; Mur, J.; Petelin, J.; Štrancar, J.; Petkovšek, R.;

1   *Title:*
2   Towards advanced retinal theranostics by adaptive two-photon compact laser source
3   (Two-photon retinal theranostics by adaptive compact laser source)
4
5   *Authors: Rok Podlipec, Jaka Mur, Jaka Petelin, Janez Strancar, Rok Petkovšek\**
6
7   *Affiliation:*
8   Rok Podlipec, Helmholtz-Zentrum Dresden-Rossendorf e.V. (HZDR), Ion Beam Center, Bautzner
9   Landstraße 400, Dresden 01328, Germany; Jožef Stefan Institute, Jamova cesta 39, SI-1000 Ljubljana,
10  Slovenia; email: rok.podlipec@ijs.si
11
12  Jaka Mur, University of Ljubljana, Faculty of Mechanical Engineering, Aškerčeva 6, SI-1000 Ljubljana,
13  Slovenia, email: jaka.mur@fs.uni-lj.si
14
15  Jaka Petelin, University of Ljubljana, Faculty of Mechanical Engineering, Aškerčeva 6, SI-1000 Ljubljana,
16  Slovenia, email: jaka.petelin@fs.uni-lj.si
17
18  Janez Strancar, Jožef Stefan Institute, Jamova cesta 39, SI-1000 Ljubljana, Slovenia; email:
19  janez.strancar@ijs.si
20
21  Rok Petkovšek, University of Ljubljana, Faculty of Mechanical Engineering, Aškerčeva 6, SI-1000
22  Ljubljana, Slovenia, email: rok.petkovsek@fs.uni-lj.si
23
24
25  *Abstract:*
26  To avoid a devastating effect of eye vision impairment on the information flow from the eye to our
27  brain, enormous effort is being put during the last decades into the development of more sensitive
28  diagnostics and more efficient therapies of retinal tissue. While morphology can be impressively
29  imaged by Optical Coherence Tomography, molecular-associated pathology information can be
30  provided almost exclusively by auto-fluorescence-based methods. Among the latter, the recently
31  developed Fluorescence lifetime imaging ophthalmoscopy (FLIO) has the potential to provide both
32  structural information and interacting pictures at the same time. The requirements for FLIO laser
33  sources are almost orthogonal to the laser sources used in phototherapy that is expected to follow-up
34  the FLIO diagnostics. To make theranostics more effective and cheaper, the complete system would
35  need to couple at least the modalities of low power high repetition rate FLIO and precision high-pulse
36  energy adjustable repetition rate phototherapy. In addition, the intermediate power high repetition
37  rate for two-photon excitation would also be desired to increase the depth resolution. In our work,
38  compact fiber-laser-based on high-speed gain-switched laser diode has been shown to achieve
39  adaptable / independently tunable repetition rate and energy per pulse allowing coupled fluorescence
40  lifetime diagnostics via two-photon excitation and phototherapy via laser-induced photodisruption on
41  a local molecular environment in a complex ex-vivo retinal tissue.
42
43  *Keywords:*
44  adaptable fiber laser; retinal tissue; theranostics; multimodal imaging; fluorescence lifetime imaging

## 1    Introduction

46  Remarkable progress in the development of advanced retinal diagnostics and therapies has been done
47  in the last decade to provide better sensitivity and specificity for detecting retinal pathologies and to
48  minimize the potential risks for damaging the targeted tissue.

49  Two large families of diagnostic methods evolved, the first based on detecting retinal fluorescence in
50  the visual part of the spectrum called Fundus Autofluorescence (FAF) [1,2] and the second based on
51  the interferometric imaging of retinal layers with NIR light called Optical Coherence Tomography (OCT)
52  [3]. Although, OCT has been developed to an impressive (even 3D) imaging tool [4], its physical
53  background, i.e. interference of the light differently scattered from different tissue structures, hinders
54  more specific identification of the physiologies or pathologies particularly present in the aging retina
55  [5]. On the contrary, FAF being sensitive to the local molecular environment [6] can provide besides
56  morphological more indicative pathology-related information. One of the latest developments based
57  on FAF is fluorescence lifetime imaging ophthalmoscopy (FLIO), implemented by Heidelberg
58  Engineering [7–9], or custom FLIO systems [10,11]. The method can monitor changes in environmental
59  parameters such as recognizing and identifying the early stages of diabetic retinopathy (DR) [8] or age-
60  related macular degeneration (AMD) [12,13] and can provide  metabolic mapping [14] unravelling
61  various macular and retinal diseases [15]. The instrumentation relies on the sub-picosecond pulsed
62  lasers with high repetition rates from few MHz [16] to few tens of MHz [17], encompassing typical
63  rates of mode-locked oscillators and fast detection electronics [18] for FLIO resolution of nearly 100 ps.

64  Current therapeutic techniques, unlike diagnostics, employ lasers with pulse duration typically orders
65  of magnitude longer, from μs for Selective Retina Therapy (SRT) [19,20] to ms for Pan Retinal
66  Photocoagulation (PRT) [21]. By low repetition rates and high energy per pulse or fluence (see the
67  schematics in Fig. 1) they provide enough thermal effect for the therapy being effective. However, due
68  to strong absorption on the highly absorbing retinal epithelium, the local dispersion of thermal effects
69  is still rather poorly defined and typically widespread causing additional complications in adjacent
70  tissue [22]. To better localize the therapeutic effect, laser pulses should in principle be faster, e.g.
71  below μs, but still with enough energy per pulse to deliver efficient therapy. Thus, the technology
72  based on nanosecond laser pulses has been recently developed with already some success in clinical
73  trials to prevent progression of the degeneration processes in AMD [23]. Furthermore, with the
74  development of femtosecond laser technology and its high ability to generate therapeutic effects with
75  markedly less energy per pulse, new possibilities emerged for the modern biomedical field. A few
76  successful clinical therapies have already been applied to corneal eye tissues, where such short pulses
77  can produce various non-linear, photo-disruptive optical effects [24].

78  To exploit the best of the described diagnostics and therapy approaches, the great challenge in the
79  field still lies in developing the adaptive system combining both, diagnostics and adaptive therapy at
80  the same time and not in a sequential way. Such theranostic principle would enable more localized
81  targeting and after-treatment-pulse diagnostics, not being possible with current systems.

82  The goal of our work was thus to overcome the current limitations of the retinal diagnostic and
83  therapeutic laser sources and boost the development of a more universal laser source concept and its
84  application. One direction is high power mode-locked fs laser technology (Ti:Sapphire), which was
85  already shown promising for diagnostics with the ability to do two-photon excitation FLIO [11,15] and
86  could as well be promising for the therapy if enough energy of high repetition pulses is accumulated.
87  However, the lasers lack the flexibility in terms of an adjustable repetition rate to be able to increase
88  energy per pulse needed for efficient therapy and are rather complex, making them particularly
89  expensive.

90  To address this challenge, we herein present the design and application of the recently developed ps
91  compact fiber laser in near-IR based on a gain switched laser diode, capable of pre-diagnostics, therapy

92    and post-diagnostics done on *ex-vivo* human retinal samples. The system enables to couple the
93    modalities of low pulse energy-high repetition rate (40 MHz) two-photon excitation for diagnostics
94    (FLIO) and high pulse energy-low repetition rate (1 kHz) for photo-disruptive induced therapy. The laser
95    system has been implemented into the modular nonlinear microscopy setup, allowing near-IR two-
96    photon excitation and fast detection for FLIO.
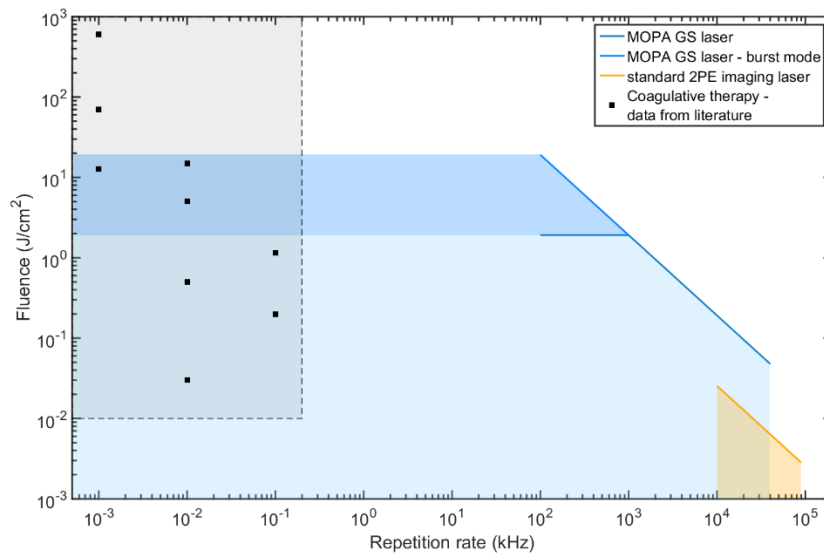


97
98    *Fig. 1. Laser parameter space. The part of the parameter space of the standard 2PE imaging lasers is denoted*
99    *with orange line and shade. The data from the literature on laser sources used in photocoagulation therapy*
100   *[19,21,25–31] is denoted with black dots emphasized inside the grey shaded area. Blue lines and shades denote*
101   *the part of the parameter space covered by the master-oscillator power-amplifier gain-switched fiber laser, with*
102   *an additional area reached by burst mode operation.*

103   ## 2    Experimental setups

104   *2.1    Laser source*

105   The master-oscillator power-amplifier (MOPA) gain-switched (GS) fiber laser source, shown in top the
106   right corner of Fig. 2, is a compact all-fiber MOPA where a gain-switched distributed-feedback (DFB)
107   laser diode ($\lambda$ = 1062 nm) is used to generate laser pulses as short as 65 ps at up to 40 MHz repetition
108   rate [32]. Key parts of the laser system are seed source and especially its driver and fiber-coupled AOM.
109   Seed source driver is capable of generating sub ns electrical pulses with high amplitude (over 50 V) at
110   a high repetition rate. These two parameters (pulse duration and amplitude) are the key in order to
111   achieve a short optical pulse duration (down to 65 ps) while driving standard DFB laser diode. To reach
112   relatively high optical pulse energy it is required to maintain adequate signal to noise (S/N) ratio of the
113   optical signal in the laser amplifiers chain at a low repetition rate. Another key component is a high-
114   speed electronic circuit that precisely synchronizes and controls both seed driver and AOM as well as
115   the laser pump system. As a result, the laser repetition rate can be set in a broad range from 40 MHz
116   to 1 kHz [33] and the output pulse energy can be set from a few nJ to approximately 15 µJ
117   independently of the repetition rate. The concept allows the laser to operate in a burst mode that
118   includes compensation of the saturation effect appearing in the amplifier chain. Consequently, the
119   energy of almost every individual pulse can be set independently within a certain time slot. Therefore,
120   the high flexibility and beam quality of this laser enable the use of the same laser for diagnostics as
121   well as for therapeutics. While laser systems with equal or even better properties exist, such as Spirit
122   by Spectra-Physics or Pharos by Light Conversion, the complexity of those sources manifests in a higher
123   up-front price and lower reliability compared to the MOPA fiber laser prototype.

124   *2.2    Multi-photon imaging system*

125 A multi-photon multimodal laser-scanning imaging system (Abberior Instruments) was used for *ex-vivo*
126 studies of human retinal tissue (see the schematic on Fig. 2). The compact imaging system is composed
127 of more fluorescence excitation units: one-photon excitation (100 ps pulsed lasers at 561 nm and
128 640 nm with repetition rate up to 80 MHz and a max output of 200 µW) and two-photon excitation
129 (MOPA GS fiber laser with 65 ps pulse length at 1062 nm with tuneable repetition rate 1 kHz - 40 MHz
130 and maximum output power of up to 15 W). Additional femtosecond Ti:Sapphire laser (Chameleon,
131 Coherent) was installed for complementary experiments of two-photon excitation. Various photon
132 counter detectors were used to detect the fluorescence: two avalanche photodiodes (APD, SPCM-
133 AQRH, Excelitas), each for the individual one-photon excitation laser with the fluorescence recording
134 within spectral bands $580 - 625$ nm and $655 - 720$ nm (filters by Semrock), and 16-channel PMT
135 detectors (PML-16-GaAsP, Hamamatsu) accompanied with a time-correlated single-photon counter
136 unit (TCSPC-SPC-150, Becker&Hickl) to acquire additional hyperspectral information of fluorescence
137 decays (tuneable 200 nm range in visible spectra). An additional band-pass filter was mounted to
138 prevent scattered or reflected light entering the detectors. Experiments were performed using a 10x
139 and 60x magnification objectives with the numerical apertures of NA = 0.3 and NA = 1.2 (both
140 Olympus). Images were performed as well with the wide-field illumination using LED source of the
141 wavelength 400 nm and CCD camera. Images using laser scanning system were obtained by fast galvo
142 scanning (Quad Scanner, Abberior Instruments) with a pixel dwell time of max. 10 µs and with more
143 accumulations over predefined scan region in case of low sample signal. Total scan time varied from
144 few seconds to few minutes.
145 Fluorescence lifetime imaging (FLIM) was recorded with TCSPC [34] synchronized with the laser
146 excitation through fast FPGA communication. The complete fluorescence decay curve was recorded in
147 each image pixel separately. In order to gain a sufficient number of detected counts and thus good S/N
148 ratio, pixel binning had to be used. To obtain a good temporal resolution of the fluorescence decay
149 when low signal counts were detected, we have chosen a conservatively higher binning in order to
150 preserve reasonable spatial resolution. Typical binning when acquiring an image with 256 x 256 pixels
151 and with sufficient signal was set to 2, while in the case of low signal a few times more. The curve
152 fitting using bi-exponential fit was done with software package SPCImage (Becker&Hickl). Fitted
153 parameters were represented with color-coded maps and accompanying histograms. Data is focused
154 on representing the average fluorescence decay time ($\tau_m$).
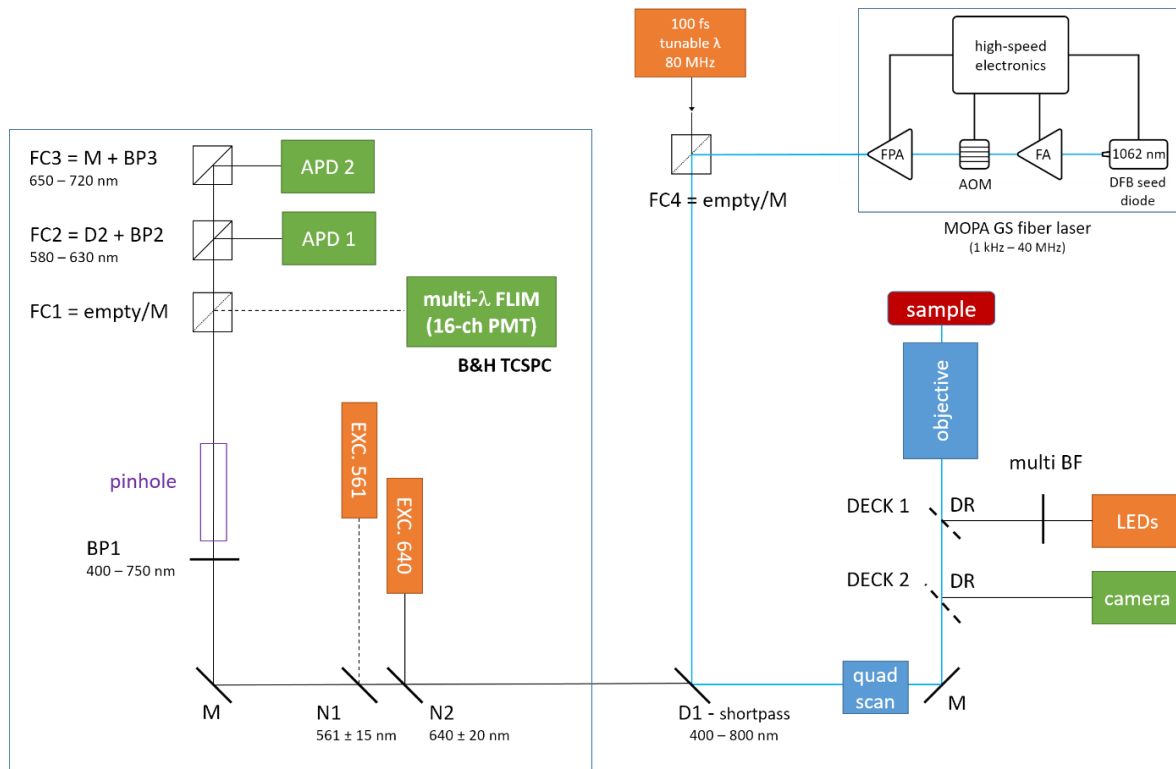
*Fig. 2. Scheme of the optical setup. Laser sources are shown in orange color, detection modules in green color. Theranostic study on the ex-vivo human retina was mainly focused on using two-photon ps laser source with tunable repetition rate (MOPA GS fiber laser) and multi-channel PMT detector with time-correlated single-photon counter (B&H). D – dichroic; DR – dichroic removable; FC – filter cube; M – mirror; BP – bandpass filter; N – notch filter.*

## 2.3 Sample preparation

Theranostics studies were performed on ex-vivo human retinal tissue. Samples were taken from the enucleated eyes of the patients with severe illness in compliance with national legislation and with the written approval of the patients. Surgical scissors and razor blade were used to separate anterior from the posterior eye segment. The posterior part of an eye excluding vitreous was placed into formalin fixative for 2 hours at the room temperature and preserved at 4 °C prior measurements.
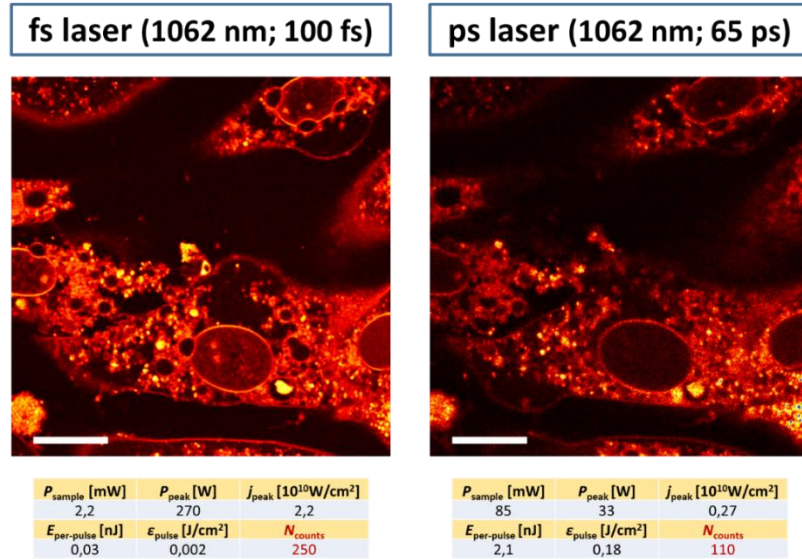
## 3 Results

### 3.1 Quantification of two-photon excitation capability of MOPA GS fiber laser

To quantify the ability for two-photon excitation to perform diagnostics, a comparison was done with the standard two-photon excitation source (mode-locked Ti:Sapphire laser; Chameleon, Coherent) (Fig. 3, left) using the same near-IR excitation wavelength 1062 nm. The study was performed on the biological sample of the *in-vitro* epithelium model composed of epithelial cell line LA4 labelled with rhodamine B based membrane probe with good two-photon absorption cross-section.

In brief, two-photon excitation is strongly dependent on the peak photon density or photon flux that can be in principal reached by the ultrashort fs to ps laser pulses. Since the electron excitation from the ground to the first excited state is done via an intermediate, very short-lived forbidden energy state, the same molecule must absorb two photons in virtually no time, which demands high photon flux. Based on the generally accepted perception, pulse durations of few tens of ps, typical for our

180    MOPA GS fiber laser, would be considered insufficient for the non-linear two-photon excitation.
181    However, it can be seen from Fig. 3, that MOPA GS fiber laser (set at a 40 MHz repetition rate) can
182    effectively excite fluorescent molecules by two-photon excitation despite an approximately 10-times
183    lower peak photon density ($j$) compared to the classical mode-locked fs laser ($t$ = 100 fs, $v$ = 80 MHz).
184    The threshold intensity for two-photon excitation for MOPA GS fiber laser (assuming on 1% of photons
185    detected; $N_{counts}/N_{pulses}$) was estimated to be approximately $j = 5*10^8$ W/cm$^2$. The comparison of the
186    experimental parameters between implemented laser systems is shown in the bottom.

187



| fs laser (1062 nm; 100 fs) | | |
| --- | --- | --- |
| $P_{sample}$ [mW] | $P_{peak}$ [W] | $j_{peak}$ [10$^{10}$W/cm$^2$] |
| 2,2 | 270 | 2,2 |
| $E_{per-pulse}$ [nJ] | $\varepsilon_{pulse}$ [J/cm$^2$] | $N_{counts}$ |
| 0,03 | 0,002 | 250 |

| ps laser (1062 nm; 65 ps) | | |
| --- | --- | --- |
| $P_{sample}$ [mW] | $P_{peak}$ [W] | $j_{peak}$ [10$^{10}$W/cm$^2$] |
| 85 | 33 | 0,27 |
| $E_{per-pulse}$ [nJ] | $\varepsilon_{pulse}$ [J/cm$^2$] | $N_{counts}$ |
| 2,1 | 0,18 | 110 |

188    Fig. 3. Quantitative comparison of *two-photon excitation using standard fs and MOPA ps pulsed laser on epithelial*
189    *cells in-vitro model labelled with 200 µl 10-5 M rhodamine based membrane probe. Image size is 500*500 pixels*
190    *with pixel dwell time of 10 µs. Focal plane moved slightly between the two acquisitions measurements. Scale bar*
191    *is 10 µm.*

192

193    *3.2    Quantification of two-photon diagnostics of MOPA GS fiber laser on ex-vivo retinal tissue*

194    Since MOPA GS fiber laser was found appropriate for two-photon excitation, we have then tested its
195    applicability on the relevant sample of *ex-vivo* retinal tissue. Besides performing conventional FAF, we
196    have tested the capability of fluorescence lifetime imaging which can provide besides morphological
197    also functional information, essential for any diagnostics.

198    FLIM analysis was done by fitting the fluorescence decay curve $f_m$ (t) with the convolution integral
199    between the instrument response function (IRF) and the double-exponential decay model $f$ (t):

200    $$f_m(t) = \int_{\tau=0}^{t} f(t)IRF(t-\tau)\,d\tau$$

201    $$f(t) = a_1 Exp(-t/\tau_1) + a_2 Exp(-t/\tau_2)$$

202    Relative amplitudes ($a_1$ and $a_2$) and the lifetimes ($\tau_1$ and $\tau_2$) of the exponential decay were used to
203    calculate the descriptive mean lifetime $\tau_m$ as:

204    $$\tau_m = \frac{a_1\tau_1 + a_2\tau_2}{a_1 + a_2}.$$

205    As shown in Fig. 4, $\tau_m$ decreases significantly at the vessel site, measured both with one-photon as well
206    as two-photon excitation using MOPA GS fiber laser. The corresponding fits of the decay curves on

207 vessel site and surrounding neural retinal tissue are shown in the inset of the Fig. 4d. $\tau_m$ at vessel site
208 was measured 500 ± 50 ps while in the surrounding neural retinal tissue 1400 ± 100 ps. From the
209 images, one can also see that the $\tau_m$ varies across the blood vessel enabling detection of the vessel
210 morphology. Finally, the results nicely show the comparison of the resolution and the sensitivity
211 between one-photon and two-photon excitation.



212
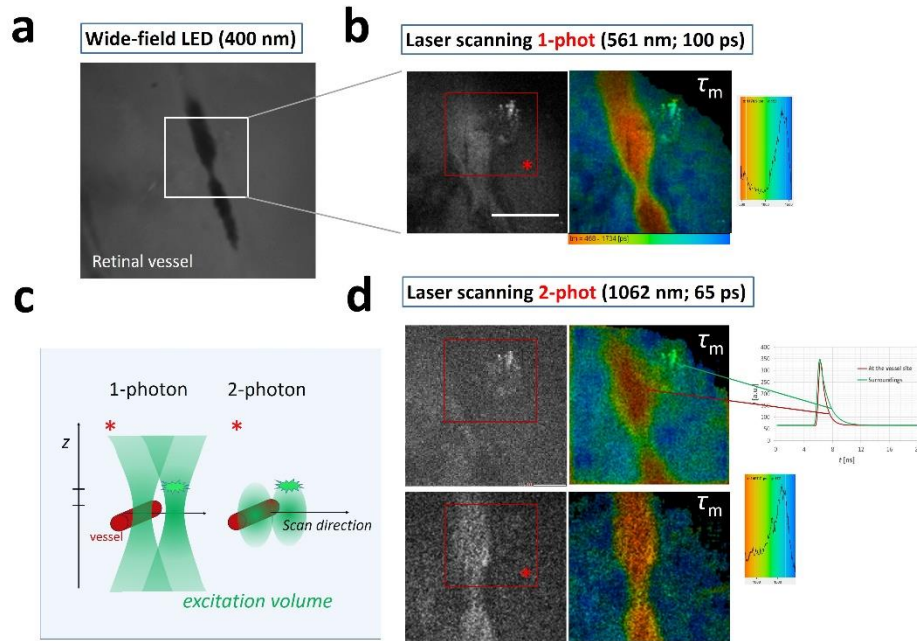
*Fig. 4. Comparison of fluorescence lifetime imaging using one-photon and two-photon laser excitation. Better*
*axial resolution was acquired using two-photon MOPA GS fiber laser with a few times lower S/N ratio. a) The*
*vessel of a fixed ex-vivo human retina imaged with wide-field LED illumination. b) The same region imaged with*
*one-photon (labelled 1-phot) laser scanning showing fluorescence lifetime using PMT detector and TCSPC unit*
*(B&H). c) Schematics of excitation volumes of one-photon and two-photon laser sources. d) Two-photon*
*fluorescence lifetime (labelled 2-phot) imaged at different axial planes using MOPA GS fiber laser. The*
*fluorescence lifetime was fitted with two components, $\tau_m$ representing the mean lifetime. Laser parameters were*
*$P_{avg}$ = 50 µW with 50 MHz repetition rate for one-photon and $P_{avg}$ = 400 mW with 40 MHz repetition rate for two-*
*photon. The image resolution is 128\*128 with 2 µm/pixel. Scale bar is 100 µm.*

222

*3.3   Quantification of two-photon diagnostics and therapy of MOPA GS fiber laser on ex-vivo retinal*
*tissue*

225 Next, MOPA GS fiber laser has been employed to do subsequent diagnostics and therapy on the same
226 sample site. Theranostics was performed on the retinal epithelial layer (RPE) on two different sites (Fig.
227 5) with different therapy settings. FLIM based pre-diagnostics was followed by an adaptive low-
228 frequency operation therapeutic laser targeted to the regions shown within white dotted rectangles.
229 By pre-diagnostics, local regions with lower measured $\tau_m$ have been attributed to higher local  melanin
230 content (marked with red color) since it is well known that melanin has up to 50% shorter lifetime than
231 surrounding lipofuscin [35]. To perform the therapy, pulse fluence was selected to induce first a
232 noticeable and second, a significant local structural damage (Fig. 5, lower experiment). 40-times higher
233 fluence was needed in comparison to diagnostics pulses, that is 0.5 J/cm$^2$ for first experiment and
234 1 J/cm$^2$ for the second. The corresponding pulse energies were 0.1 µJ and 0.2 µJ. By post-diagnostics
235 analysis, areas that were affected by the therapeutic pulses inside the therapy region have changed
236 structurally as well as functionally shown by FLIM analysis. The difference is more pronounced in the
237 experiment shown in the bottom (Fig. 5, 3rd column). The main changes are seen through the local

238 shifts in $\tau_m$, presented in histograms (Fig. 5, 4th column)and through the partial disappearance of the
239 RPE region, the effect known for a successful selective retinal therapy (SRT) that can be a consequence
240 of either the cell death [36] or the local laser ablation [37].

241
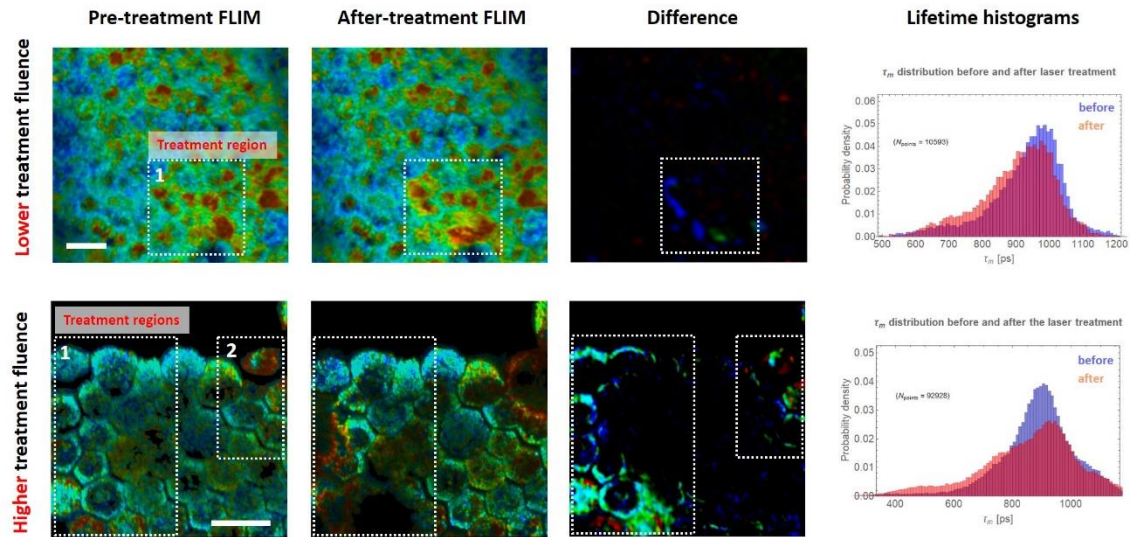


242

243 *Fig. 5. Diagnostics and therapy of targeted fixed human RPE using the same MOPA GS fiber two-photon laser*
244 *using low and high magnification objectives. The regions of laser treatment are denoted with white rectangles.*
245 *The pre- and post-diagnostics was analyzed by calculating $\tau_m$. Sites affected by treatment pulses) are clearly*
246 *visible as seen on the presented difference. The average laser power was the same for diagnostics and treatment*
247 *($P_{avg} \approx 100mW$ and $P_{avg} \approx 200mW$), while the fluence and the energy per pulse were 40-times higher for the*
248 *treatment ($\varepsilon_{pulse} \approx 0.5$ J/cm2; $E_{pulse} \approx 0.1$ µJ and $\varepsilon_{pulse} \approx 1$ J/cm2; $E_{pulse} \approx 0.2$ µJ). The total treatment time at each*
249 *region was 30 s. The total diagnostics time was 100 s. Scale bar is 20 µm.*

250

## 4    Discussion

252 The results presented in Fig. 4 nicely show the comparison of two-photon MOPA GS fiber laser with
253 the one-photon diode laser regarding the resolution and the sensitivity. MOPA GS fiber laser can
254 achieve almost the same spatial resolution of the fluorescence lifetime $\tau_m$ compared to one-photon
255 excitation (see the vessel region on Fig. 4b and d). However, significantly higher S/N ratio was acquired
256 using one-photon excitation, originating in a much higher photon absorption probability, compared to
257 the two-photon nonlinear process [38]. Thus, the energy of the two-photon laser necessary to acquire
258 relevant FLIM images with the similar sensitivity of retinal vessels was relatively high, but still below
259 the threshold for altering the tissue or the therapeutic effect.

260 On the other hand, two-photon laser enabled the detection of the retinal structures at higher depths
261 and with better axial resolution (see the marked red region). We could locate the vessel and the nearby
262 pathology clearly at different axial planes, not observed with the one-photon laser, where both
263 structures seem to be in the same axial plane (Fig. 4b and d). This is attributed to more localized
264 excitation volume schematically represented in Fig. 4c.

265 With both lasers, $\tau_m$ at vessel site was measured 500 ± 50 ps while in the surrounding neural retinal
266 tissue 1400 ± 100 ps. Low $\tau_m$ at the vessel site is mainly due to hemoglobin presence which contributes
267 to short fluorescence decay component $\tau_1$, calculated 270 ± 30 ps, which is in a good agreement with
268 the results published recently [39]. Measured lifetime components in the surrounding neural retinal
269 tissue, $\tau_1 = 600 ± 100$ ps and $\tau_2 = 2500 ± 300$ ps, on the other hand partially match with the ones in the

270    published data [35]. $\tau_2$ agrees very nicely with the known lifetimes of the most abundant endogenous
271    molecules, such as FAD, collagen, and lipofuscin, while $\tau_1$ was measured longer compared to the
272    literature. This could be attributed to changes in the intrinsic fluorescence properties due to chemical
273    fixation that can cause an increase in fluorescence lifetime [40,41]. However, the fixation of the tissues
274    preserves metabolic contrast, the relationship of the lifetimes, and thus the functional information.

275    The presented applicability of the adaptive MOPA GS fiber laser for retinal diagnostics was further
276    tested for potential applicability in retinal therapy. The results are summarized in Fig. 5, where pre-
277    diagnostics, therapy and post-diagnostics using different modalities of the laser were done on retinal
278    RPE on two different sites with different laser treatment settings. The therapeutic laser parameters
279    were set in such a way to create noticeable (first experiment) to significant structural damage (second
280    experiment). A 40-times higher fluence compared to the diagnostic pulse was needed to induce
281    damage, which was achieved by lowering the laser frequency to 1 MHz. The effect of the increased
282    energy per pulse was observed locally within the chosen treatment region on the few sites with the
283    higher average melanin content than in surroundings.  .

284    The local change in $\tau_m$ shows that the effect is highly dependent on the local molecular environment,
285    rich in waste material (lipofuscin) and essentially, absorbing melanin specific for retinal pigment
286    epithelium. Furthermore, the effect causes local reduction of the autofluorescence signal as well, that
287    was particularly shown for short therapy laser pulses before [36]. Due to the orders of magnitude
288    shorter laser pulses that deliver lower energy doses, a negligible thermal effect was induced as
289    opposed to the known thermal photocoagulation therapies [42]. High peak powers reaching $10^{11}$
290    $W/cm^2$ irradiance rather introduced local plasma mediated ablation [43] on the sites with high melanin
291    content. Melanin can thus indirectly or directly contribute to the changes in fluorescence lifetime –
292    the effect, which has already been documented [44]. It is almost surprising to note, that melanin, a
293    complex mixture of different biopolymers derived from tyrosine, known as a broadband absorber, can
294    even express a complex emission decay with fluorescence decay ranging from ps to ns [17]. Another
295    explanation for the decrease in the lifetime in those local regions would be a photo-disruptive effect
296    of laser on lipofuscin rich molecules with longer lifetimes that lose part of the fluorescence.

297    We have shown that both functional diagnostics using FLIM and local therapy inducing photo-ablation
298    can be done by the same laser source. However, the study was performed on the fixated *ex-vivo* retina
299    thus questioning the relevance of the used theranostics parameters for *in-vivo*. It was previously shown
300    that fixation can cause a change in the scattering coefficient and retardance to the tissue but the
301    absorption coefficient remains unchanged [45]. We can thus expect that therapeutic parameters
302    would not be significantly changed when targeting non-fixated tissues.

303    To sum up, the developed MOPA GS fiber laser has fulfilled several demands for the technology being
304    applicable in future theranostics:

305        1) Capability of operating at a high repetition rate and sufficient fluence (orange shade of parameter
306        space in Fig. 1) in a controlled, scanning-like approach [46] to collect diagnostics signal in order to
307        localize the following therapeutic pulses (Fig. 4 and Fig. 5);

308        2) Energy per pulse as well as repetition rate were adaptable depending on the mode of action.
309        Diagnostics mode used low power and high repetition rate (orange shade of parameter space in
310        Fig. 1) and in therapy mode vice versa (blue shades of parameter space in Fig. 1);

311        3) By merging the two modes of action – diagnostics and therapy, the system reduces the need of
312        more sophisticated eye-tracking systems;

313        4) The system is cost-effective, which is beneficial once introduced into clinics.

314

## 5   Conclusions

Compact fiber-laser-based on high-speed gain-switched DFB laser diode has been shown to achieve adaptable / independently tuneable repetition rate and energy per pulse allowing coupled two-photon fluorescence lifetime diagnostics and photo-induced ablation therapy of local molecular environment in a complex retinal tissue. Several demands for potential applicability in future theranostics were met and discussed thoroughly. This was the first example of implementing a cost-effective adaptive laser source to show efficient simultaneous two-photon based functional diagnostics and therapy on the relevant human *ex-vivo* retinal sample. However, further laser development is needed before application in clinical trials that could eventually enable advanced theranostics of retinal tissues *in-vivo*.

### References

[1]   F.C. Delori, C.K. Dorey, G. Staurenghi, O. Arend, D.G. Goger, J.J. Weiter, In vivo fluorescence of the ocular fundus exhibits retinal pigment epithelium lipofuscin characteristics, Invest. Ophthalmol. Vis. Sci. 36 (1995) 718–729.

[2]   A. von Rückmann, F.W. Fitzke, A.C. Bird, Distribution of fundus autofluorescence with a scanning laser ophthalmoscope, Br J Ophthalmol. 79 (1995) 407–412. https://doi.org/10.1136/bjo.79.5.407.

[3]   A.F. Fercher, K. Mengedoht, W. Werner, Eye-length measurement by interferometry with partially coherent light, Opt. Lett., OL. 13 (1988) 186–188. https://doi.org/10.1364/OL.13.000186.

[4]   W. Drexler, U. Morgner, R.K. Ghanta, F.X. Kärtner, J.S. Schuman, J.G. Fujimoto, Ultrahigh-resolution ophthalmic optical coherence tomography, Nature Medicine. 7 (2001) 502–507. https://doi.org/10.1038/86589.

[5]   J. Marshall, The ageing retina: Physiology or pathology, Eye. 1 (1987) 282–295. https://doi.org/10.1038/eye.1987.47.

[6]   J. Sparrow, T. Duncker, J.R. Sparrow, T. Duncker, Fundus Autofluorescence and RPE Lipofuscin in Age-Related Macular Degeneration, Journal of Clinical Medicine. 3 (2014) 1302–1321. https://doi.org/10.3390/jcm3041302.

[7]   J. Teister, A. Liu, D. Wolters, N. Pfeiffer, F.H. Grus, Peripapillary fluorescence lifetime reveals age-dependent changes using fluorescence lifetime imaging ophthalmoscopy in rats, Experimental Eye Research. 176 (2018) 110–120. https://doi.org/10.1016/j.exer.2018.07.008.

357 [8] J. Schmidt, S. Peters, L. Sauer, D. Schweitzer, M. Klemm, R. Augsten, N. Müller, M. Hammer,
358 Fundus autofluorescence lifetimes are increased in non-proliferative diabetic retinopathy, Acta
359 Ophthalmologica. 95 (2017) 33–40. https://doi.org/10.1111/aos.13174.

360 [9] L. Sauer, R.H. Gensure, M. Hammer, P.S. Bernstein, Fluorescence Lifetime Imaging
361 Ophthalmoscopy: A Novel Way to Assess Macular Telangiectasia Type 2, Oph Retina. 2 (2018)
362 587–598. https://doi.org/10.1016/j.oret.2017.10.008.

363 [10] D. Schweitzer, L. Deutsch, M. Klemm, S. Jentsch, M. Hammer, S. Peters, J. Haueisen, U.A. Müller,
364 J. Dawczynski, Fluorescence lifetime imaging ophthalmoscopy in type 2 diabetic patients who
365 have no signs of diabetic retinopathy, JBO, JBOPFO. 20 (2015) 061106.
366 https://doi.org/10.1117/1.JBO.20.6.061106.

367 [11] J.A. Feeks, J.J. Hunter, Adaptive optics two-photon excited fluorescence lifetime imaging
368 ophthalmoscopy of exogenous fluorophores in mice, Biomed. Opt. Express, BOE. 8 (2017) 2483–
369 2495. https://doi.org/10.1364/BOE.8.002483.

370 [12] C. Dysli, R. Fink, S. Wolf, M.S. Zinkernagel, Fluorescence Lifetimes of Drusen in Age-Related
371 Macular Degeneration, Invest. Ophthalmol. Vis. Sci. 58 (2017) 4856–4862.
372 https://doi.org/10.1167/iovs.17-22184.

373 [13] L. Sauer, C.B. Komanski, A.S. Vitale, E.D. Hansen, P.S. Bernstein, Fluorescence Lifetime Imaging
374 Ophthalmoscopy (FLIO) in Eyes With Pigment Epithelial Detachments Due to Age-Related
375 Macular Degeneration, Invest Ophthalmol Vis Sci. 60 (2019) 3054–3063.
376 https://doi.org/10.1167/iovs.19-26835.

377 [14] D. Schweitzer, S. Schenke, M. Hammer, F. Schweitzer, S. Jentsch, E. Birckner, W. Becker, A.
378 Bergmann, Towards metabolic mapping of the human retina, Microscopy Research and
379 Technique. 70 (2007) 410–419. https://doi.org/10.1002/jemt.20427.

380 [15] C. Dysli, S. Wolf, M.Y. Berezin, L. Sauer, M. Hammer, M.S. Zinkernagel, Fluorescence lifetime
381 imaging ophthalmoscopy, Progress in Retinal and Eye Research. 60 (2017) 120–143.
382 https://doi.org/10.1016/j.preteyeres.2017.06.005.

383 [16] A. Periasamy, P. Wodnicki, X.F. Wang, S. Kwon, G.W. Gordon, B. Herman, Time-resolved
384 fluorescence lifetime imaging microscopy using a picosecond pulsed tunable dye laser system,
385 Review of Scientific Instruments. 67 (1996) 3722–3731. https://doi.org/10.1063/1.1147139.

386 [17] A. Ehlers, I. Riemann, M. Stark, K. König, Multiphoton fluorescence lifetime imaging of human
387 hair, Microscopy Research and Technique. 70 (2007) 154–161.
388 https://doi.org/10.1002/jemt.20395.

389 [18] B. Leskovar, C.C. Lo, P.R. Hartig, K. Sauer, Photon counting system for subnanosecond
390 fluorescence lifetime measurements, Review of Scientific Instruments. 47 (1976) 1113–1121.
391 https://doi.org/10.1063/1.1134827.

392 [19] J. Roider, S.H.M. Liew, C. Klatt, H. Elsner, E. Poerksen, J. Hillenkamp, R. Brinkmann, R. Birngruber,
393 Selective retina therapy (SRT) for clinically significant diabetic macular edema, Graefes Arch Clin
394 Exp Ophthalmol. 248 (2010) 1263–1272. https://doi.org/10.1007/s00417-010-1356-3.

395 [20] E. Seifert, J. Tode, A. Pielen, D. Theisen-Kunde, C. Framme, J. Roider, Y. Miura, R. Birngruber, R.
396 Brinkmann, Selective retina therapy: toward an optically controlled automatic dosing, J Biomed
397 Opt. 23 (2018) 1–12. https://doi.org/10.1117/1.JBO.23.11.115002.

398 [21] S. Al-Hussainy, P.M. Dodson, J.M. Gibson, Pain response and follow-up of patients undergoing
399 panretinal laser photocoagulation with reduced exposure times, Eye. 22 (2008) 96–99.
400 https://doi.org/10.1038/sj.eye.6703026.

401 [22] S.V. Reddy, D. Husain, Panretinal Photocoagulation: A Review of Complications, Seminars in
402 Ophthalmology. 33 (2018) 83–88. https://doi.org/10.1080/08820538.2017.1353820.

403 [23] R.H. Guymer, Z. Wu, L.A.B. Hodgson, E. Caruso, K.H. Brassington, N. Tindill, K.Z. Aung, M.B.
404 McGuinness, E.L. Fletcher, F.K. Chen, U. Chakravarthy, J.J. Arnold, W.J. Heriot, S.R. Durkin, J.J.
405 Lek, C.A. Harper, S.S. Wickremasinghe, S.S. Sandhu, E.K. Baglin, P. Sharangan, S. Braat, C.D. Luu,
406 Laser Intervention in Early Stages of Age-Related Macular Degeneration Study Group,
407 Subthreshold Nanosecond Laser Intervention in Age-Related Macular Degeneration: The LEAD
408 Randomized Controlled Clinical Trial, Ophthalmology. 126 (2019) 829–838.
409 https://doi.org/10.1016/j.ophtha.2018.09.015.

410 [24] W.R. Calhoun, I.K. Ilev, Effect of therapeutic femtosecond laser pulse energy, repetition rate, and
411 numerical aperture on laser-induced second and third harmonic generation in corneal tissue,
412 Lasers Med Sci. 30 (2015) 1341–1346. https://doi.org/10.1007/s10103-015-1726-5.

413 [25] Z. Hu, H. Zhang, A. Mordovanakis, Y.M. Paulus, Q. Liu, X. Wang, X. Yang, High-precision, non-
414 invasive anti-microvascular approach via concurrent ultrasound and laser irradiation, Scientific
415 Reports. 7 (2017) 40243. https://doi.org/10.1038/srep40243.

416 [26] J.P.M. Wood, O. Shibeeb, M. Plunkett, R.J. Casson, G. Chidlow, Retinal Damage Profiles and
417 Neuronal Effects of Laser Treatment: Comparison of a Conventional Photocoagulator and a
418 Novel 3-Nanosecond Pulse Laser, Invest. Ophthalmol. Vis. Sci. 54 (2013) 2305–2318.
419 https://doi.org/10.1167/iovs.12-11203.

420 [27] Y. Takatsuna, S. Yamamoto, Y. Nakamura, T. Tatsumi, M. Arai, Y. Mitamura, Long-term
421 therapeutic efficacy of the subthreshold micropulse diode laser photocoagulation for diabetic
422 macular edema, Jpn J Ophthalmol. 55 (2011) 365–369. https://doi.org/10.1007/s10384-011-
423 0033-3.

424 [28] G. Schuele, H. Elsner, C. Framme, J. Roider, R. Birngruber, R. Brinkmann, Optoacoustic real-time
425 dosimetry for selective retina treatment, JBO, JBOPFO. 10 (2005) 064022.
426 https://doi.org/10.1117/1.2136327.

427 [29] Y.M. Paulus, A. Jain, H. Nomoto, C. Sramek, R.F. Gariano, D. Andersen, G. Schuele, L.-S. Leung, T.
428 Leng, D. Palanker, SELECTIVE RETINAL THERAPY WITH MICROSECOND EXPOSURES USING A
429 CONTINUOUS LINE SCANNING LASER, RETINA. 31 (2011) 380.
430 https://doi.org/10.1097/IAE.0b013e3181e76da6.

431 [30] R.R. Anderson, J.A. Parrish, Selective photothermolysis: precise microsurgery by selective
432 absorption of pulsed radiation, Science. 220 (1983) 524–527.
433 https://doi.org/10.1126/science.6836297.

434 [31] W.T. Ham, R.C. Williams, H.A. Mueller, D. Guerry, A.M. Clarke, W.J. Geeraets, Effects of Laser
435 Radiation on the Mammalian Eye*†, Transactions of the New York Academy of Sciences. 28
436 (1966) 517–526. https://doi.org/10.1111/j.2164-0947.1966.tb02368.x.

437 [32] J. Petelin, B. Podobnik, R. Petkovšek, Burst shaping in a fiber-amplifier chain seeded by a gain-
438 switched laser diode, Appl. Opt., AO. 54 (2015) 4629–4634.
439 https://doi.org/10.1364/AO.54.004629.

440 [33] M. Šajn, J. Petelin, V. Agrež, M. Vidmar, R. Petkovšek, DFB diode seeded low repetition rate fiber
441     laser system operating in burst mode, Optics & Laser Technology. 88 (2017) 99–103.
442     https://doi.org/10.1016/j.optlastec.2016.09.006.

443 [34] W. Becker, Advanced Time-Correlated Single Photon Counting Techniques, Springer-Verlag,
444     Berlin Heidelberg, 2005. //www.springer.com/la/book/9783540260479 (accessed September 6,
445     2018).

446 [35] D. Schweitzer, S. Schenke, M. Hammer, F. Schweitzer, S. Jentsch, E. Birckner, W. Becker, A.
447     Bergmann, Towards metabolic mapping of the human retina, Microsc. Res. Tech. 70 (2007) 410–
448     419. https://doi.org/10.1002/jemt.20427.

449 [36] J.P.M. Wood, M. Plunkett, V. Previn, G. Chidlow, R.J. Casson, Nanosecond pulse lasers for retinal
450     applications, Lasers Surg Med. 43 (2011) 499–510. https://doi.org/10.1002/lsm.21087.

451 [37] B. Považay, R. Brinkmann, M. Stoller, R. Kessler, Selective Retina Therapy, in: J.F. Bille (Ed.), High
452     Resolution Imaging in Microscopy and Ophthalmology: New Frontiers in Biomedical Optics,
453     Springer International Publishing, Cham, 2019: pp. 237–259. https://doi.org/10.1007/978-3-030-
454     16638-0_11.

455 [38] W. Denk, J.H. Strickler, W.W. Webb, Two-photon laser scanning fluorescence microscopy,
456     Science. 248 (1990) 73–76. https://doi.org/10.1126/science.2321027.

457 [39] I. Saytashev, R. Glenn, G.A. Murashova, S. Osseiran, D. Spence, C.L. Evans, M. Dantus,
458     Multiphoton excited hemoglobin fluorescence and third harmonic generation for non-invasive
459     microscopy of stored blood, Biomed Opt Express. 7 (2016) 3449–3460.
460     https://doi.org/10.1364/BOE.7.003449.

461 [40] NAD(P)H fluorescence lifetime measurements in fixed biological tissues. - PubMed - NCBI, (n.d.).
462     https://www.ncbi.nlm.nih.gov/pubmed/31553966 (accessed March 17, 2020).

463 [41] D. Schweitzer, E.R. Gaillard, J. Dillon, R.F. Mullins, S. Russell, B. Hoffmann, S. Peters, M. Hammer,
464     C. Biskup, Time-resolved autofluorescence imaging of human donor retina tissue from donors
465     with significant extramacular drusen, Invest. Ophthalmol. Vis. Sci. 53 (2012) 3376–3386.
466     https://doi.org/10.1167/iovs.11-8970.

467 [42] B. Považay, R. Brinkmann, M. Stoller, R. Kessler, Selective Retina Therapy, in: J.F. Bille (Ed.), High
468     Resolution Imaging in Microscopy and Ophthalmology: New Frontiers in Biomedical Optics,
469     Springer International Publishing, Cham, 2019: pp. 237–259. https://doi.org/10.1007/978-3-030-
470     16638-0_11.

471 [43] G. Keiser, Light-Tissue Interactions, in: G. Keiser (Ed.), Biophotonics: Concepts to Applications,
472     Springer, Singapore, 2016: pp. 147–196. https://doi.org/10.1007/978-981-10-0945-7_6.

473 [44] E. Dimitrow, I. Riemann, A. Ehlers, M.J. Koehler, J. Norgauer, P. Elsner, K. König, M. Kaatz,
474     Spectral fluorescence lifetime detection and selective melanin imaging by multiphoton laser
475     tomography for melanoma diagnosis, Experimental Dermatology. 18 (2009) 509–515.
476     https://doi.org/10.1111/j.1600-0625.2008.00815.x.

477 [45] M.F.G. Wood, N. Vurgun, M.A. Wallenburg, I.A. Vitkin, Effects of formalin fixation on tissue
478     optical polarization properties, Phys. Med. Biol. 56 (2011) N115–N122.
479     https://doi.org/10.1088/0031-9155/56/8/N01.

480  [46] M.A. Mainster, G.T. Timberlake, R.H. Webb, G.W. Hughes, Scanning laser ophthalmoscopy.
481       Clinical applications, Ophthalmology. 89 (1982) 852–857. https://doi.org/10.1016/s0161-
482       6420(82)34714-4.

483